THE ASTRONOMICAL JOURNAL, 121:1607–1613, 2001 March

PRECISE MASSES FOR WOLF 1062 AB FROM *HUBBLE SPACE TELESCOPE* INTERFEROMETRIC ASTROMETRY AND MCDONALD OBSERVATORY RADIAL VELOCITIES[1]

G. F. BENEDICT,[2] B. E. MCARTHUR,[2] O. G. FRANZ,[3] L. H. WASSERMAN,[3] T. J. HENRY,[4] T. TAKATO,[7] I. V. STRATEVA,[14] J. L. CRAWFORD,[15] P. A. IANNA,[13] D. W. MCCARTHY,[5] E. NELAN,[6] W. H. JEFFERYS,[7] W. VAN ALTENA,[8] P. J. SHELUS,[2] P. D. HEMENWAY,[9] R. L. DUNCOMBE,[10] D. STORY,[11] A. L. WHIPPLE,[11] A. J. BRADLEY,[12] AND L. W. FREDRICK[13]

Received 2000 August 28; accepted 2000 December 1

ABSTRACT

We present an analysis of astrometric data from Fine Guidance Sensor 3 (FGS 3), a white-light interferometer on *HST*, and of radial velocity data from two ground-based campaigns. We model the astrometric and radial velocity measurements simultaneously to obtain parallax, proper motion, and component masses for Wolf 1062 (Gl 748; M3.5 V). To derive the mass fraction, we relate FGS 3 fringe scanning observations of the science target to a reference frame provided by fringe tracking observations of a surrounding star field. We obtain an absolute parallax ($\pi_{abs} = 98.0 \pm 0.4$ mas) yielding $M_A = 0.379 \pm 0.005\ M_\odot$ and $M_B = 0.192 \pm 0.003\ M_\odot$, high-quality component masses with errors of only 1.5%.

Key words: astrometry — binaries: general — stars: individual (Wolf 1062) — stars: distances — stars: fundamental parameters — stars: late-type — techniques: interferometric

1. INTRODUCTION

This is a paper in a series presenting accurate masses of stars on the lower main sequence, where the complex interplay of luminosity, age, and mass can be explored. The dependence of intrinsic brightness upon mass, the mass-luminosity relation (MLR), is applicable to many areas of astronomy. After the H-R diagram, it is perhaps the most important relationship in stellar astronomy, because the entire evolution of a star depends on mass. The MLR remains poorly determined for M dwarfs, by far the dominant population of the Galaxy in both numbers (>70%) and stellar mass contribution (>40%; Henry 1998), and it is critical in distinguishing stars from brown dwarfs. Below 0.1 $M_\odot$, an accurate mass determination can convincingly turn a brown dwarf candidate into a bona fide brown dwarf.

Wolf 1062 is an M dwarf binary with one component suspected to be in the 20-20-20 sample defined by Henry et al. (1999) as having $d \leq 20$ pc, ($\pi \geq 0\farcs05$), $M \leq 0.2\ M_\odot$, and orbital period $P \leq 20$ yr. With the motivation that the secondary is one of the few objects that promises an accurate dynamic mass less than 0.2 $M_\odot$, we obtained astrometric observations at 15 epochs with *HST* and radial velocities at 15 epochs with which to derive a precise parallax and masses. Our astrometric observations were obtained with Fine Guidance Sensor 3 (FGS 3), a two-axis, white-light interferometer aboard *HST*. Most of our radial velocities were obtained at McDonald Observatory. Three velocities of component A came from Marcy & Benitz (1989).

Table 1 provides aliases and physical parameters for Wolf 1062. We time-tag our data with a modified Julian Date, MJD = JD − 2,444,000.5, and abbreviate milliarcseconds, mas, throughout.

Bradley et al. (1991) provide an overview of the FGS 3 instrument, and Benedict et al. (1999) describe the fringe-tracking (POS mode) astrometric capabilities of FGS 3 and typical data acquisition and reduction strategies. Our response to the added astrometric complication of resolved orbital motion is discussed in Benedict et al. (2000b). Details concerning the treatment of fringe-scanning (TRANS mode) data are available in a paper presenting a preliminary relative orbit for Wolf 1062 (Franz et al. 1998). To summarize, TRANS data are used to obtain relative positions of the A and B components; POS data are used to obtain the photocenter position of component A relative to a reference frame.

Franz et al. (1999) present a definitive relative orbit obtained from fringe-scanning (TRANS) data. The present analysis utilizes only the 15 (of 17 total) TRANS measurements in which the secondary was resolved on both FGS axes. We combine these with 15 epochs of fringe-tracking (POS) measurements relative to a reference frame and with radial velocities to obtain a parallax, absolute orbits, and masses. POS data were not acquired at the first two epochs

[1] Based on observations made with the NASA/ESA *Hubble Space Telescope*, obtained at the Space Telescope Science Institute, which is operated by the Association of Universities for Research in Astronomy, Inc., under NASA contract NAS 5-26555.

[2] McDonald Observatory, University of Texas at Austin, Austin, TX 78712-1083.
[3] Lowell Observatory, 1400 West Mars Hill Road, Flagstaff, AZ 86001.
[4] Department of Physics and Astronomy, Georgia State University, Atlanta, GA 30303-3083.
[5] Steward Observatory, University of Arizona, 933 North Cherry Avenue, Tucson, AZ 85721.
[6] Space Telescope Science Institute, 3700 San Martin Drive, Baltimore, MD 21218.
[7] Department of Astronomy, University of Texas at Austin, Austin, TX 78712.
[8] Department of Astronomy, Yale University, P.O. Box 208101, New Haven, CT 06520.
[9] Graduate School of Oceanography, Department of Physics, University of Rhode Island, Kingston, RI 02881.
[10] Department of Aerospace Engineering, University of Texas at Austin, Austin, TX 78712.
[11] Jackson and Tull, Aerospace Engineering Division, 7375 Executive Place, Suite 200, Seabrook, MD 20706.
[12] Spacecraft System Engineering Services, P.O. Box 91, Annapolis Junction, MD 20706.
[13] Department of Astronomy, University of Virginia, P.O. Box 3818, Charlottesville, VA 22903.
[14] Department of Astrophysical Science, Princeton University, Princeton, NJ 08544-1001.
[15] Applied Research Laboratories, University of Texas at Austin, Austin, TX 78713-8029.

TABLE 1

WOLF 1062 = GL 748 = HIP 94349 = LHS 472 = G 22−18

Parameter	Value	Reference
V.....	11.12 ± 0.04	Leggett (1992)
$B-V$	1.51 ± 0.05	Leggett (1992)
Spectral Type.....	M3.5 V	Henry et al. (1999)

of TRANS data. In contrast to our recent work on Gl 791.2 (Benedict et al. 2000b), we include ground-based radial velocities in our analysis. The constraint provided by the requirement that astrometry and radial velocities describe the same physical system improves the accuracy of our result.

2. WOLF 1062 ASTROMETRIC REFERENCE FRAME

Figure 1 shows the distribution in FGS 3 pickle coordinates of the 15 sets of three reference-star measurements for the Wolf 1062 reference frame. The circular pattern is impressed by the requirement that *HST* roll to keep its solar panels fully illuminated throughout the year. At each epoch we measured reference stars 2 and 4 once and reference star 3 twice for a total of 60 reference-star observations.

2.1. *Astrometric Model*

From these data we determine the scale, rotation, and offset "plate constants" relative to an arbitrarily adopted constraint epoch (the so-called master plate) for each observation set. The Wolf 1062 reference frame contains only three stars. Hence, we constrain the scales along X and Y to equality and the two axes to orthogonality. The consequences of this choice are minimal. For example, imposing these constraints on the Barnard's Star astrometry discussed in Benedict et al. (1999) results in an unchanged parallax and increases the error by 0.1 mas, compared to a full six-parameter model.

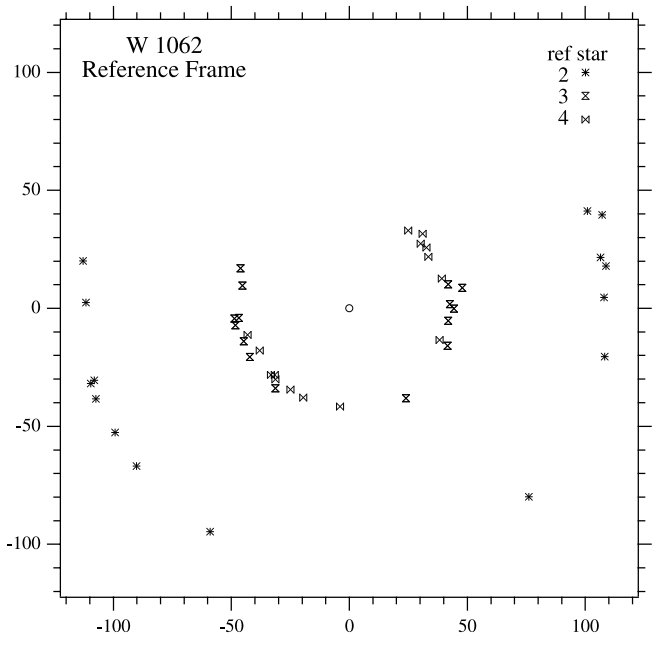

FIG. 1.—Wolf 1062 and reference-frame observations in FGS 3 pickle coordinates. Symbols identify each star listed in Table 2.

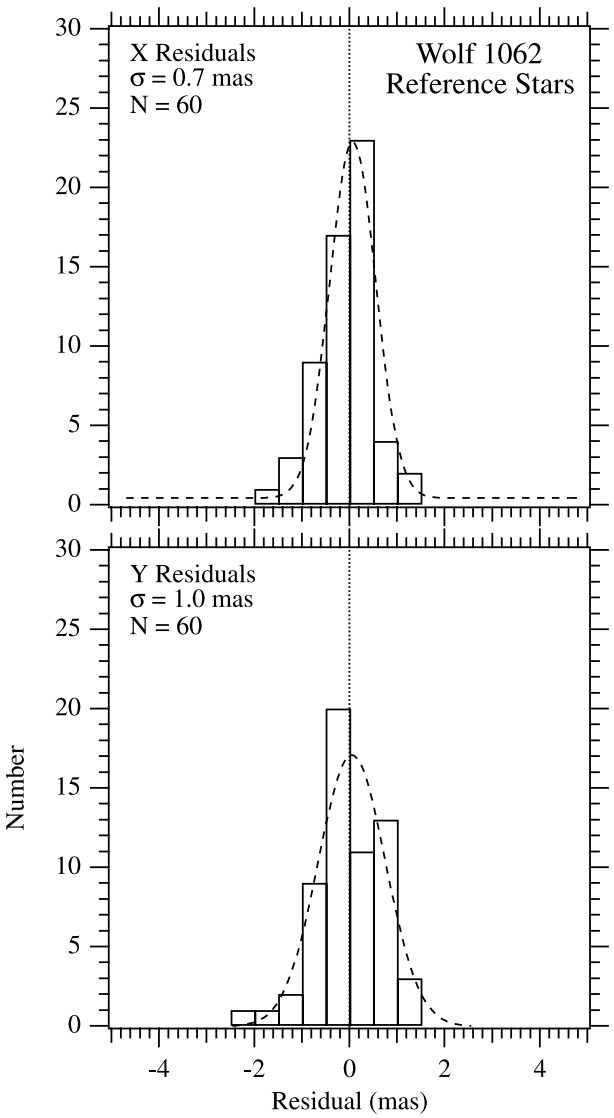

FIG. 2.—Histograms of X and Y residuals obtained from modeling the Wolf 1062 reference frame with eqs. (1) and (2). Distributions are fitted with Gaussians.

The astrometric residuals for an initial solution constraining the parallax and proper motions of the three reference stars to zero values showed that one reference star had nonzero proper motion. We therefore include the effects of reference star 4 parallax (π) and proper motion (μ). Our reference frame model becomes in terms of standard coordinates

$$\xi = aX + bY + c - P_x * \pi - \mu_x * t\,, \quad (1)$$

$$\eta = -bX + aY + f - P_y * \pi - \mu_y * t\,, \quad (2)$$

where a, b, c and f are the plate constants obtained from the reference frame, and t is time. We constrain $\mu = 0$ and $\pi = 0$ for reference stars 2 and 3. The master-plate orientation to the sky is obtained from ground-based astrometry (Monet 1998) with uncertainties in the field orientation $\pm 0.^{\circ}3$. We obtain the parallax factors P_x and P_y from a JPL Earth orbit predictor (Standish 1990), upgraded to version DE405. From USNO-A2.0 photometry (Monet 1998), calibrated as discussed in Benedict et al. 2000a and presented in

Table 2, we see that the colors of the reference stars and the target are all fairly red. Hence, we apply no corrections for lateral color (Benedict et al. 1999).

2.2. *Assessing Reference Frame Residuals*

The optical field angle distortion calibration (McArthur et al. 1997) reduces as-built *HST* telescope and FGS 3 distortions of $\sim 1''$ to below 2 mas over much of the FGS 3 field of regard. From histograms of the astrometric residuals (Fig. 2) we conclude that we have obtained correction at the ~ 1 mas level in the region available at all *HST* rolls (an inscribed circle centered on the pickle-shaped FGS field of regard). The resulting reference frame "catalog" in ξ and η standard coordinates (Table 2) was determined with $\langle \sigma_\xi \rangle = 0.5$ and $\langle \sigma_\eta \rangle = 0.6$ mas.

To determine if there might be unmodeled—but possibly correctable—systematic effects at the 1 mas level, we plotted the Wolf 1062 reference frame X and Y residuals against a number of spacecraft, instrumental, and astronomical parameters. These included (X, Y) position within the pickle, radial distance from the pickle center, reference-star V magnitude and $B-V$ color, and epoch of observation. We saw no obvious trends, other than an expected increase in positional uncertainty of the reference-star magnitude.

3. RADIAL VELOCITIES

Our radial velocity data have two sources. We obtain three early epochs of absolute radial velocities from Marcy & Benitz (1989). To this we add radial velocity measurements (Table 3) at 12 epochs, obtained with the McDonald 2.1 m telescope and Sandiford Cassegrain echelle spectrograph (McCarthy et al. 1993). The McDonald data were reduced using the standard IRAF (Tody 1993) ECHELLE package tools, including FXCORR. Treating Wolf 1062 as a double-lined spectroscopic binary, we obtained velocities for both components at all but one orbital phase.

4. WOLF 1062 PARALLAX AND ORBITS FROM ASTROMETRY AND RADIAL VELOCITIES

4.1. *Correction to Absolute Parallax*

Before we can determine the absolute masses of the A and B components, we need the distance, which we obtain by means of a parallax relative to our reference stars. Every small-field astrometric technique requires a correction from relative to absolute parallax because the reference frame stars have an intrinsic parallax. We adopt the corrections discussed and presented in the Yale parallax catalog (van Altena, Lee, & Hoffleit 1995, § 3.2, Fig. 2, hereafter YPC95). We enter Figure 2 of YPC95, with the Wolf 1062 Galactic latitude, $b = -3\overset{\circ}{.}3$ and average magnitude for the reference frame, $\langle V_{\rm ref} \rangle = 13.7$, and obtain a correction to absolute of 1.2 ± 0.2 mas. The error for the correction is determined by comparing the spectrophotometric parallaxes of the reference frames of the low Galactic latitude science targets discussed in Harrison et al. (1999), McArthur et al. (1999), and Benedict et al. (1999) with the YPC95 corrections.

TABLE 2

WOLF 1062 REFERENCE FRAME

Reference Star	V	$B-V$	ξ (arcsec)	η (arcsec)	μ_X (arcsec yr^{-1})	μ_Y (arcsec y^{-1})	π (arcsec)
2[a]	12.8	0.7	0.0000 ± 0.0006	0.0000 ± 0.0007	0	0	0
3	14.1	1.4	-59.2177 ± 0.0004	-30.8548 ± 0.0006	0	0	0
4	14.2	0.7	-76.0673 ± 0.0005	-7.8994 ± 0.0007	-0.0131 ± 0.0005	0.0034 ± 0.0006	0.0002 ± 0.0004

[a] R.A. 288°.087967, decl. 2.898281; J2000.0.

TABLE 3

RADIAL VELOCITY OBSERVATIONS OF WOLF 1062 AND RESIDUALS

MJD	Source[a]	Phase	Radial Velocity (A)[b] (km s^{-1})	Residual (A) (km s^{-1})	Radial Velocity (B)[b] (km s^{-1})	Residual (B) (km s^{-1})
46,627.5	MB	0.699	-42.42 ± 0.30	-0.23	...	...
46,665.5	MB	0.741	-42.41 ± 0.30	0.06	...	...
46,899.5	MB	0.000	-41.75 ± 0.30	0.11	...	...
49,960.65	McD	0.395	-33.96 ± 0.16	-0.18	-50.49 ± 0.77	0.30
50,214.42	McD	0.676	-41.81 ± 0.06	0.21	-34.21 ± 0.39	0.64
50,364.96	McD	0.843	-42.64 ± 0.05	0.00	-33.75 ± 0.64	-0.11
50,403.59	McD	0.886	-42.64 ± 0.11	-0.12	-33.55 ± 0.82	0.31
50,530.01	McD	0.026	-41.73 ± 0.14	-0.01	-35.58 ± 0.36	-0.17
50,584.56	McD	0.087	-41.10 ± 0.06	0.07	-36.69 ± 0.22	-0.20
50,723.09	McD	0.240	-38.74 ± 0.09	0.11	-40.98 ± 0.09	0.00
51,028.80	McD	0.579	-39.54 ± 0.07	0.00	...	...
51,079.69	McD	0.636	-41.37 ± 0.06	-0.03	-36.21 ± 0.42	-0.06
51,138.58	McD	0.701	-42.22 ± 0.12	0.06	-34.25 ± 0.93	0.09
51,313.70	McD	0.895	-42.53 ± 0.06	-0.03	-33.88 ± 0.49	0.04
51,466.12	McD	0.064	-41.43 ± 0.05	-0.04	-35.94 ± 0.22	0.11
$\langle \lvert \text{res} \rvert \rangle$[c]	...	...	...	0.08	...	0.14

[a] (MB) Marcy & Benitz 1989; (McD) McDonald Observatory.

[b] The McD radial velocities have been adjusted to the Marcy system (absolute velocities) using the two γ's derived from the simultaneous solution.

[c] For $N = 15$.

4.2. *POS Mode Photocenter Corrections*

For binary stars the FGS transforms the images of the two components into two overlapping fringes. For perfect fringes and component separations greater than the resolution of *HST* at $\lambda = 580$ nm, about 40 mas, the presence of a companion should have little effect on the component A position obtained from the fringe-zero crossing. However, FGS 3 does not produce perfect fringes (Franz et al. 1998). Given the uncorrected *HST* point-spread function (PSF) for the FGSs (they are not in the COSTAR path), we must apply photocenter-type corrections (see, e.g., van de Kamp 1967). The measurement of the position of the brighter component of a blended image will be biased toward the fainter. Because the detector has two orthogonal axes, the separation along each interferometer axis, not the total separation on the sky, determines the photocenter correction. For any arbitrary *HST* orientation, components A and B can have separations along the FGS axes from 0.0 mas to the actual full separation. For example, observation set 17 in Table 4 has a total separation, ρ_A, of 176.2 mas. Resolved on each interferometer axis, $\Delta x = 52.3$ mas and $\Delta y = 168.2$ mas.

Simulations were done to characterize the effect of the secondary on the position derived for the primary for separations of less than 200 mas. First, we obtained a position (the central zero-crossing point of the fringe) derived from a fringe scan of a single star of appropriate color. Then, a companion with $\Delta V = 1.80$ (the magnitude difference between the components in this system) was placed at many separations along each axis and a combined fringe obtained. As can be seen in Figure 1 of Franz et al. (1998), the interferometer response functions are not symmetric about the zero crossing, particularly for the X fringe. Hence, the simulation requires that the companion be placed on either side of the primary. Fitting each synthetic binary TRANS scan as a single star will quantify the effect of the companion on the measured position of the primary.

The results of this simulation are shown in Figure 3. Classically, the correction always increases the separation of the two components. In general we see this for both axes. However, such is the perversity of the X-axis fringe that at times the correction works in the opposite sense. Photocenter corrections are negligible for separations greater than 120 mas for either axis. As expected from the differing X- and Y-fringe morphologies, the corrections are strongly asymmetric along the X axis, peaking at ~ -5 mas at a separation of -35 mas. The measures with corrections applied are listed in Table 4.

4.3. *Simultaneous Estimation of Parallax, Proper Motion, Mass Ratio, and Orbit Parameters for Wolf 1062*

We apply the transformations (eqs. [1] and [2]) to the Wolf 1062 POS (corrected for photocenter effects) and TRANS measurements. We fold in the radial velocity measurements, solving for relative parallax, proper motion, and orbital motion of both components simultaneously. The model now becomes

$$\xi = aX + bY + c - P_x * \pi - \mu_x * t - \mathrm{ORBIT}_x\,, \quad (3)$$

$$\eta = -bX + aY + f - P_y * \pi - \mu_y * t - \mathrm{ORBIT}_y\,. \quad (4)$$

ORBIT is a function of the traditional astrometric and radial velocity orbital elements, listed in Table 6.

For the simultaneous solution, we constrain equality for the eccentricities (e) and longitudes of periastron (ω) of the two component orbits. We also constrain the position angle of the line of nodes (Ω) for the component A and B orbits to differ by 180°. The period (P), the epoch of passage through periastron in years (T), the eccentricity (e), and the angle in the plane of the true orbit between the line of nodes and the major axis (ω) are constrained to be equal in the radial velocity and two modes of astrometry. Only radial velocity provides information with which to determine the half-amplitudes (K_1, K_2) and the systemic velocity (γ). Combining radial velocity observations from different sources is simple with GAUSSFIT (Jefferys, Fitzpatrick, & McArthur 1988), which has the ability to solve for two separate γ-values simultaneously with the other orbital parameters. We easily mix absolute velocities from Marcy & Benitz (1989) with the relative velocities from our own program.

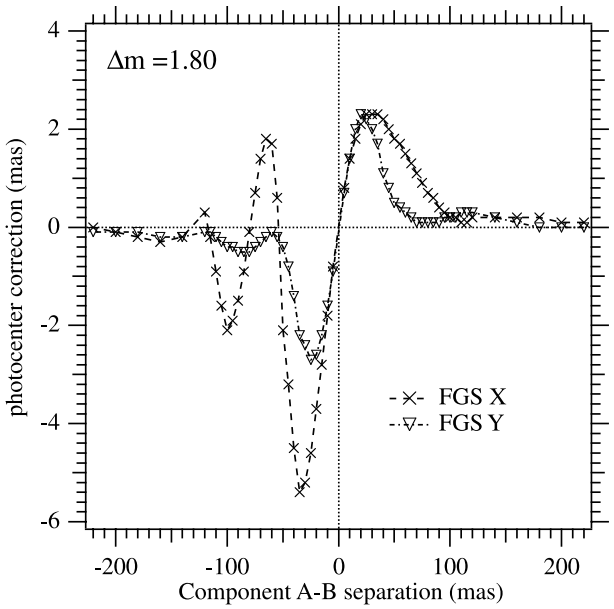

FIG. 3.—Fringe-tracking (POS) photocenter corrections in milliarcseconds for various component separations along the FGS X and Y axes. Y corrections are, as expected, more symmetric and smaller.

The relationship between the two astrometric modes (POS and TRANS) and the radial velocity is enforced by the constraint

$$\frac{\alpha_A \sin i}{\pi_{\mathrm{abs}}} = \frac{PK_1(1-e^2)^{1/2}}{2\pi 4.7405} \quad (5)$$

(Pourbaix & Jorissen 2000), where quantities derived only from astrometry (parallax, π_{abs}, primary perturbation orbit size, α_A, and inclination, i) are on the left and quantities derivable from both (the period, P and eccentricity, e) or from radial velocities only (the radial velocity amplitude for the primary, K_1) are on the right.

The results of this simultaneous solution are as follows. The absolute parallax and the proper motion are presented in Table 5 (errors are 1 σ). The final, formal, parallax uncertainty includes the estimated error in the correction to absolute, 0.2 mas, combined in quadrature with the relative parallax error. Our precision has improved our knowledge of the parallax by a factor of 6, compared with *Hipparcos* and YPC95. Table 6 contains the relative orbital parameters with formal (1 σ) uncertainties. For comparison we include our previous relative orbit from Franz et al. (1999). Residuals for the POS, TRANS, and radial velocity obser-

TABLE 4

POS Observations of Wolf 1062A and Residuals

Observation Set	MJD	ρ_A (mas)	θ (deg)	$\Delta\rho_A$ (mas)	$\Delta\theta$ (deg)	$\rho_A\Delta\theta$ (mas)
3	49,926.481	32.6	53.3	−0.5	7.1	4.0
	49,926.499	32.9	53.3	0.1	6.0	3.4
4	49,956.507	31.7	33.1	2.0	0.5	0.3
	49,956.525	31.2	33.1	1.6	0.0	0.0
5	49,970.380	29.6	23.8	0.2	−3.5	−1.8
	49,970.397	29.7	23.8	0.2	−4.4	−2.3
6	49,995.646	28.9	6.7	−0.8	−5.5	−2.8
	49,995.664	28.4	6.7	−0.9	−1.8	−0.9
7	50,031.034	25.8	339.2	0.7	−0.7	−0.3
	50,031.052	25.0	339.2	0.1	0.7	0.3
8	50,164.733	38.0	213.1	0.0	−2.0	−1.3
	50,164.751	39.0	213.1	−1.0	−1.8	−1.2
9	50,193.220	45.7	203.7	−0.9	1.8	1.4
	50,193.238	46.1	203.7	−1.2	1.4	1.2
10	50,230.679	52.2	194.9	2.1	−2.3	−2.1
	50,230.697	52.2	194.9	2.2	−2.3	−2.1
11	50,246.763	53.4	191.8	−1.1	0.7	0.6
	50,246.780	53.1	191.8	−0.6	0.3	0.3
12	50,351.175	66.6	176.4	0.2	−1.7	−2.0
	50,351.196	66.0	176.4	−0.4	−1.4	−1.6
13	50,359.081	67.4	175.4	−0.9	−0.4	−0.5
	50,359.102	67.3	175.4	−1.0	−0.1	−0.1
14	50,413.362	67.6	168.8	0.1	1.3	1.5
	50,413.384	68.1	168.8	0.2	0.7	0.9
15	50,529.867	63.2	154.2	−0.2	−1.0	−1.1
	50,529.888	62.5	154.2	0.5	−1.6	−1.7
16	50,554.807	61.0	150.6	−0.8	0.7	0.7
	50,554.828	61.0	150.6	−0.8	0.6	0.7
17	50,592.184	58.1	144.5	0.8	−0.4	−0.4
	50,592.205	58.4	144.5	0.3	0.2	0.2
$\langle \lvert res \rvert \rangle$[a]	...	...	...	0.8	1.8	1.3

[a] For $N = 30$.

vations are given in Tables 3, 4, and 7 respectively. Figure 4 contains all radial velocity measures, radial velocity residuals, and the predicted velocity curve from the simultaneous solutions. Figure 5 presents the astrometric residuals and the derived perturbation orbit for component A. Figure 6 provides component A and component B orbits. The vectors connecting the components all pass through the center of mass with an average positional scatter of less than 2 mas.

TABLE 5

Wolf 1062 Parallax and Proper Motion

Parameter	Value
HST study duration (yr)	1.8
Number of observation sets	15
Reference stars $\langle V \rangle$	13.7 ± 0.25
Reference stars $\langle B-V \rangle$	0.9 ± 0.4
HST relative parallax (mas)	96.8 ± 0.3
Correction to absolute (mas)	1.2 ± 0.2
HST absolute parallax (mas)	98.0 ± 0.4
Hipparcos absolute parallax (mas)	98.6 ± 2.7
YPC95 absolute parallax (mas)	99.8 ± 2.4
HST proper motion (mas yr^{-1})	1856.5 ± 1.0
In position angle (deg)	106.9 ± 0.1
Hipparcos proper motion (mas yr^{-1})	1863.3 ± 3.4
In position angle (deg)	106.2 ± 0.4
YPC95 proper motion (mas yr^{-1})	1801.0
In position angle (deg)	105.8

5. COMPONENT MASSES

Our orbit solutions (Table 6) and associated absolute parallax (Table 5) provide an orbit semimajor axis a in AU, from which we can determine the system mass through Kepler's Law. Given P and a, we solve the expression

$$a^3/P^2 = M_A + M_B = M_{\rm tot} . \quad (6)$$

We find $M_{\rm tot} = 0.571 \pm 0.008\ M_\odot$. At each instant in the orbits of the two components around the common center of mass,

$$M_A/M_B = \alpha_B/\alpha_A , \quad (7)$$

a relationship that contains only one observable, the perturbation orbit size α_A. We calculate instead the mass fraction

$$f = M_B/(M_A + M_B) = \alpha_A/(\alpha_A + \alpha_B) = \alpha_A/a , \quad (8)$$

where $\alpha_B = a - \alpha_A$. This parameter compares the two quantities directly obtained from the observations: the perturbation orbit size (α_A from POS mode) and the relative orbit size (a from TRANS mode). Both quantities are shown in Figure 6 and listed in Table 6. From these we derive a mass fraction of 0.3358 ± 0.0021. Equations (6), (7), and (8)

TABLE 6

Wolf 1062 Orbits

Parameter	Component A	Component B	Relative[a]
α (mas)	49.9 ± 0.3	98.6 ± 0.4	...
P (days)	901.77 ± 0.47	...	900.9223 ± 3.0639
P (yr)	2.4689 ± 0.0013	...	2.4664 ± 0.0075
T_0	1995.8623 ± 0.0010	...	1995.8646 ± 0.0037
e	0.4519 ± 0.0013	...	0.4532 ± 0.0041
i (deg)	130.8 ± 0.3	...	131.5 ± 0.8
Ω (deg)	0.7 ± 0.1	180.7 ± 0.1	178.8 ± 0.6
ω (deg)	27.3 ± 0.1	...	26.5 ± 1.0
K_1 (km s^{-1})	5.20 ± 0.06	...	...
K_2 (km s^{-1})	10.08 ± 0.19	...	...
γ (km s^{-1})	−39.5 ± 0.1	...	...
a (mas)	148.5 ± 0.3	...	147.95 ± 0.9
a (AU)	1.515 ± 0.007	...	...
f	0.3358 ± 0.0021	...	...

[a] Franz et al. 1999.

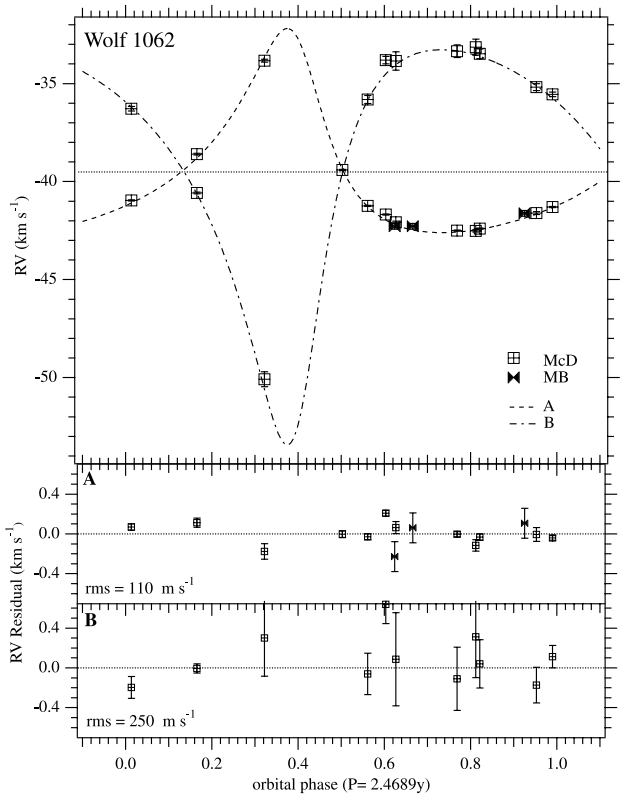

FIG. 4.—*Top*: radial velocity measurements from Marcy & Benitz (1989; MB) and the present study (McD), phased to the orbital period determined from a combined solution including astrometry and radial velocity. The lines are velocities predicted from the orbital parameters derived in the combined solution. *Middle* and *bottom*: radial velocity residuals from the combined solution for component A and B, respectively. The error bars on the residuals are the original measurement errors (1 σ).

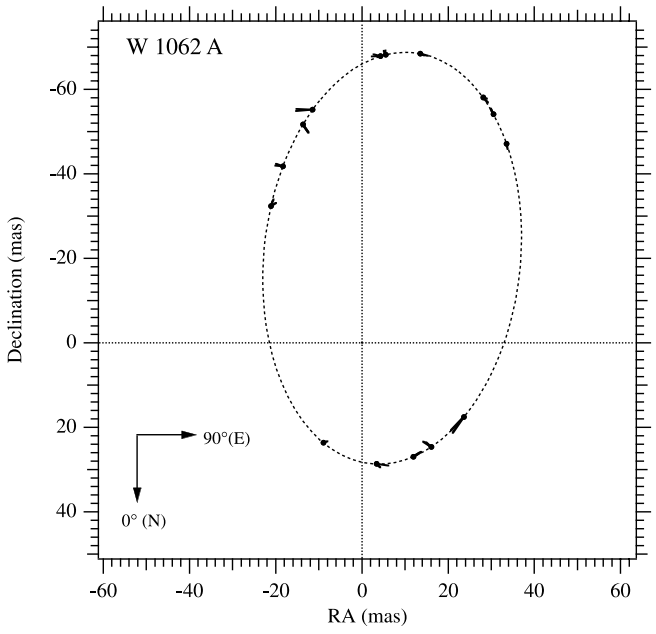

FIG. 5.—Perturbation orbit for Wolf 1062 A. Elements are found in Table 6. Circles are predicted positions at each epoch of observation. Residual vectors are plotted for each observation, two at each epoch (see Table 4).

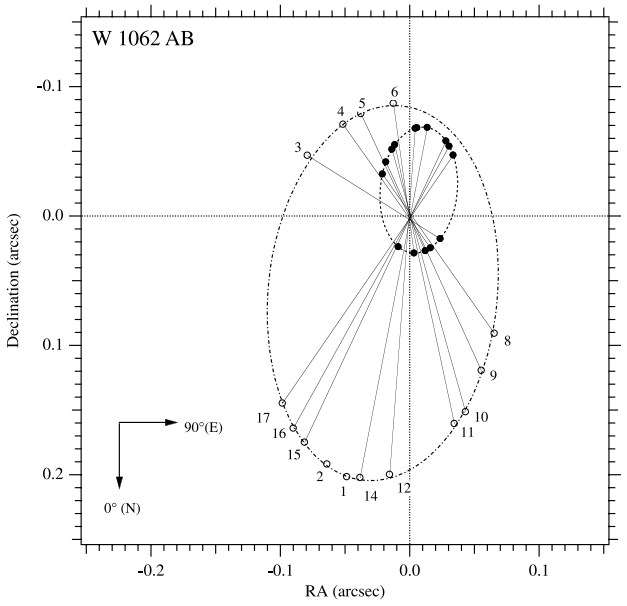

FIG. 6.—Wolf 1062A (*filled circles*; POS measurements) and Wolf 1062B (*open circles*; TRANS detections). Component B positions are labeled with their corresponding observation set numbers (Table 7). All observations, both POS and TRANS, as well as component A and B radial velocities, were used to derive the orbital elements in Table 6. Sets 1 and 2 had TRANS data only. Sets 7 and 13 were resolved only along one axis and hence are not plotted.

yield $M_A = 0.379 \pm 0.005\ M_\odot$ and $M_B = 0.192 \pm 0.003\ M_\odot$, indicating that component B is of very low mass and is a valuable member of the 20-20-20 sample with a mass error of only 1.5%.

6. WOLF 1062A AND B ON THE MLR

With the component masses determined, we require the component absolute magnitudes to place these stars on the MLR. We use the photometry from Leggett (1992), $V_{\rm tot} = 11.12 \pm 0.03$, and a $\Delta V = 1.83 \pm 0.03$ from Henry et al. (1999) to derive component magnitudes $V_A = 11.30 \pm 0.03$ and $V_B = 13.13 \pm 0.04$. With our parallax, $\pi_{\rm abs} = 98.0 \pm 0.4$

TABLE 7

TRANS OBSERVATIONS OF WOLF 1062B AND RESIDUALS

Observation Set	MJD	ρ_A (mas)	θ (deg)	$\Delta\rho_A$ (mas)	$\Delta\theta$ (deg)	$\rho_A \Delta\theta$ (mas)
1	49,534.723	207.5	346.5	−0.2	0.1	0.4
2	49,578.078	201.5	341.6	0.8	−0.3	−1.0
3	49,926.490	96.5	239.4	−4.6	−2.9	−5.0
4	49,956.516	87.7	216	−0.1	0.0	0.0
5	49,970.389	87.7	205.6	0.0	1.1	1.7
6	49,995.655	89.7	188.3	−1.5	1.4	2.1
8	50,164.742	111.9	35.7	−0.4	−0.9	−1.7
9	50,193.229	130.5	24.9	0.9	0.1	0.2
10	50,230.688	158.3	15.9	−1.0	−0.2	−0.5
11	50,246.388	162.9	12.1	1.1	0.4	1.1
12	50,351.186	199.5	355.6	0.9	1.4	4.7
14	50,413.373	204.3	349.3	1.6	0.1	0.2
15	50,529.878	193	335	−0.1	−0.3	−0.9
16	50,554.818	187.9	331.2	−1.0	0.0	−0.1
17	50,592.195	176.2	325.8	−1.4	−0.5	−1.5
$\langle \lvert \text{res} \rvert \rangle^a$....	...	...	...	1.0	0.6	1.4

[a] For $N = 15$.

TABLE 8

WOLF 1062 COMPONENT MASSES AND M_V

Parameter	Value
M_{tot} ($M_\odot$).....	0.571 ± 0.008
M_A ($M_\odot$)	0.379 ± 0.005
M_B ($M_\odot$)	0.192 ± 0.003
M_{VA}	11.26 ± 0.03
M_{VB}	13.09 ± 0.04

mas, we find $M_{VA} = 11.26 \pm 0.03$ and $M_{VB} = 13.09 \pm 0.04$. For this very nearby system we have assumed no absorption ($A_V = 0$). Neither does a parallax of this precision require correction for Lutz-Kelker bias (Lutz & Kelker 1973) in the derived absolute magnitudes. We collect all derived mass and absolute magnitude values in Table 8.

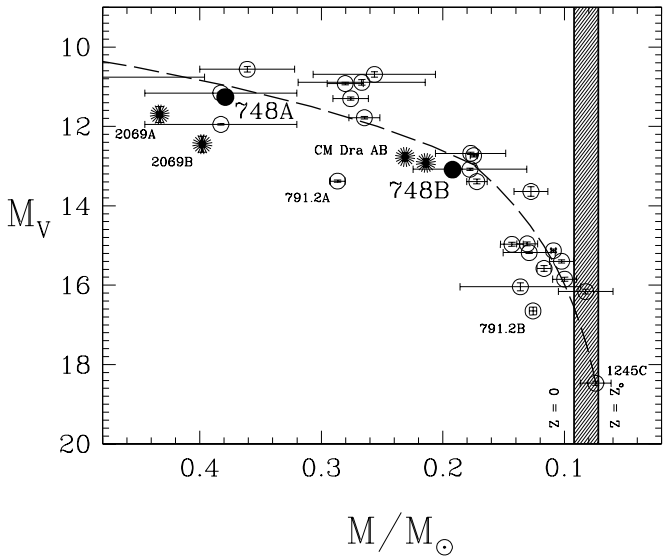

FIG. 7.—Mass-luminosity diagram, showing the components of Wolf 1062 as filled circles, the sizes of which indicate the mass errors. A few other stars of interest are labeled, including the four components of the GJ 2069 (Delfosse et al. 1999) and CM Dra (Metcalfe et al. 1996) eclipsing binary systems (*asterisks*) and the recent determinations for Gl 791.2 AB by this group (Benedict et al. 2000b). Also labeled is GJ 1245C, still the lowest mass object for which an accurate dynamic mass has been determined. The curve is the empirical mass-luminosity relation from Henry & McCarthy (1993) down to 0.18 $M_\odot$ and from Henry et al. (1999) at lower masses. The shaded region with borders at 0.092 and 0.072 $M_\odot$ marks the main-sequence minimum mass range for objects with zero to solar metallicity.

Components A and B lie on the MLR as shown in Figure 7. The lower–main-sequence relation is from Henry et al. (1999). The higher-mass section ($M > 0.2\ M_\odot$) is from Henry & McCarthy (1993).

7. CONCLUSIONS

1. We obtained POS observations of the low-mass binary Wolf 1062 over a 1.8 yr time span and TRANS observations of that system over a 2.9 yr span with *HST* FGS 3. These yield an absolute parallax $\pi_{abs} = 98.0 \pm 0.4$ mas with an external error better than 1%.

2. Fringe-tracking (POS) observations of the primary, component A, provide a well-determined perturbation orbit, once photocenter effects are corrected.

3. Fringe scans (TRANS) combined with POS observations provide a mass fraction of 0.3358 ± 0.0021 relative to an astrometric reference frame. TRANS data also provide a ΔV of 1.83 ± 0.03 (Henry et al. 1999).

4. We obtain masses precise to 1.5%: $M_{tot} = 0.571 \pm 0.008\ M_\odot$, $M_A = 0.379 \pm 0.005\ M_\odot$, and $M_B = 0.192 \pm 0.003\ M_\odot$.

5. The system magnitude, the component magnitude difference ΔV, and our parallax provide component absolute magnitudes, $M_{VA} = 11.26 \pm 0.03$ and $M_{VB} = 13.09 \pm 0.04$.

6. These masses and absolute magnitudes assist in defining the lower–main-sequence MLR. The primary provides one of the few high-quality masses between 0.2 and 0.5 $M_\odot$. The secondary lies below 0.2 $M_\odot$, the crucial region where age begins to play a significant role in the flux of stars.

Support for this work was provided by NASA through grants GTO NAG 5-1603, GO-06036.01-94A and GO-07491.01-97A from the Space Telescope Science Institute, which is operated by the Association of Universities for Research in Astronomy, Inc., under NASA contract NAS 5-26555. We thank Linda Abramowicz-Reed, now at Raytheon-Danbury, for her unflagging and expert instrumental support over the last 15 years. Finally, we thank an anonymous referee who made several suggestions that resulted in an improved paper.

REFERENCES

Benedict, G. F., et al. 1999, AJ, 118, 1086
———. 2000a, AJ, 119, 2382
Benedict, G. F., McArthur, B. E., Franz, O. G., Wasserman, L. H., & Henry, T. J. 2000b, AJ, 120, 1106
Bradley, A., Abramowicz-Reed, L., Story, D., Benedict, G., & Jefferys, W. 1991, PASP, 103, 317
Delfosse, X., Forveille, T., Mayor, M., Burnet, M., & Perrier, C. 1999, A&A, 341, L63
Franz, O. G., et al. 1998, AJ, 116, 1432
———. 1999, in ASP Conf. Ser. 194, Working on the Fringe: Optical and IR Interferometry from Ground and Space, ed. S. Unwin & R. Stachnik (San Francisco: ASP), 28
Harrison, T. E., McNamara, B. J., Szkody, P., McArthur, B. E., Benedict, G. F., Klemola, A. R., & Gilliland, R. L. 1999, ApJ, 515, L93
Henry, T. J. 1998, in ASP Conf. Ser. 134, Brown Dwarfs and Extrasolar Planets, ed. R. Rebolo, E. L. Martín, & M. R. Zapatero-Osorio (San Francisco: ASP), 28
Henry, T. J., Franz, O. G., Wasserman, L. H., Benedict, G. F., Shelus, P. J., Ianna, P. A., Kirkpatrick, J. D., & McCarthy, D. W., Jr. 1999, ApJ, 512, 864
Henry, T. J., & McCarthy, D. W., Jr. 1993, AJ, 106, 773
Jefferys, W., Fitzpatrick, M. J., & McArthur, B. 1987, Celest. Mech., 41, 39
Leggett, S. K. 1992, ApJS, 82, 351
Lutz, T. E., & Kelker, D. H. 1973, PASP, 85, 573
Marcy, G. W., & Benitz, K. J. 1989, ApJ, 344, 441
McArthur, B., Benedict, G. F., Jefferys, W. H., & Nelan, E. 1997, in The 1997 *HST* Calibration Workshop, ed. S. Casertano, R. Jedrzejewski, C. D. Keyes, & M. Stevens (Baltimore: STScI), 472
McArthur, B. E., et al. 1999, ApJ, 520, L59
McCarthy, J. K., Sandiford, B. A., Boyd, D., & Booth, J. 1993, PASP, 105, 881
Metcalfe, T. S., Mathieu, R. D., Latham, D. W., & Torres, G. 1996, ApJ, 456, 356
Monet, D. G. 1998, BAAS, 193, 120.03
Pourbaix, D., & Jorissen, A. 2000, A&AS, 145, 161
Standish, E. M., Jr. 1990, A&A, 233, 252
Tody, D. 1993, in ASP Conf. Ser. 52, Astronomical Data Analysis Software and Systems II, ed. R. J. Hanisch, R. J. V. Brissenden, & J. Barnes (San Francisco: ASP), 173
van Altena, W. F., Lee, J. T., & Hoffleit, E. D. 1995, The General Catalogue of Trigonometric Stellar Parallaxes (4th ed.; New Haven: Yale Univ. Obs.) (YPC95)
van de Kamp, P. 1967, Principles of Astrometry (San Francisco: Freeman)